# OBSERVATIONS AND MODELING OF TRANSVERSE FINGER BARS

Anneke ten Doeschate[1], Francesca Ribas[2], Huib de Swart[1], Gerben Ruessink[1] and Daniel Calvete[2]

**Abstract**

The formation of transverse finger bars at Surfers Paradise, in the Gold Coast, East Australia, has been characterized with four years of time-exposure video images. These bars are relatively small, attached to the inner bar, and have an oblique orientation. They are observed during 24% of the study period, in patches of 3 to 15 bars, with an average lifetime of 5 days and a mean wavelength of 32 m. The bars were present during intermediate energy wave conditions. Bar crests typically point towards the direction of the incoming waves, i.e., they are up-current oriented. A morphodynamic self-organization model, which describes the feedback between waves, currents and bed evolution, has been applied to investigate the Gold Coast finger bars. Realistic positive feedback leading to formation of the observed bars only occurs if the re-suspension of sediment due to roller-induced turbulence is included. The alongshore current strength also plays an important role; the offshore root mean square wave height must be larger than 0.3 m and the wave incidence angle larger than $20^o$ (at 18-m depth). Preliminary model-data comparison indicates that the modeled bar shape characteristics (wavelength, up-current orientation) and the wave conditions leading to bar formation agree with data, whilst the modeled crest orientation and migration rate are larger than the observed ones.

**Key words:** transverse finger bars, video remote sensing, linear stability analysis, Gold Coast

## 1. Introduction

Sandy beaches often display pronounced morphological features, such as crescentic sandbars and rip channels. In this contribution we focus on the less well known transverse finger bars, relatively small, shore-oblique bars that are attached to an inner sand bar or to the shoreline. Observations from Duck, USA (Konicki and Holman, 2000) and Noordwijk, Netherlands (Ribas and Kroon, 2007) indicate finger bars to be relatively rare features with a typical alongshore wavelength of several tens of meters. Bars migrate at rates up to a few tens of meters per day in the direction of the longshore current. Ribas and Kroon (2007) also correlated the wavelength, crest orientation and migration rate of Noordwijk bars with quantities (e.g., wave radiation stress component $S_{xy}$) derived from hourly wave conditions (measured at an 18-m depth buoy). Crests of finger bar were obliquely oriented from the shore-normal in the up-flow direction (`up-current orientation'). Wave conditions detected in Noordwijk during bar presence were characterized as intermediate waves (root mean square wave height, $H^{off} \approx 0.75$ m) with large angles of incidence with respect to the shore-normal ($\theta^{off} \approx 50^o$).

Finger bars can form as a result of morphodynamic self-organization in the nearshore, i.e. due to the feedbacks between hydrodynamics (waves and currents) and bed evolution (Ribas et al., 2012). The alongshore current, induced by obliquely incident breaking waves, deflects over the crest of the finger bars mainly due to frictional torques. This flow deflection, together with a depth-integrated sediment concentration that increases in the landward direction, promotes growth of finger bars with an up-current orientation. Ribas et al. (2012) used a model that includes the dynamics of surface rollers and the corresponding turbulence-induced sediment re-suspension. Including these processes was essential to accurately reproduce the longshore current and wave height profiles and to successfully explain the formation of finger bars at Noordwijk (Ribas et al., 2011a; 2012) and at Duck (Ribas et al., 2011b). Regarding the formation of finger bars, rollers are essential because the corresponding induced turbulent

[1]Institute for Marine and Atmorpheric research Utrecht, Utrecht University, The Netherlands. a.m.m.tendoeschate@students.uu.nl, h.e.deswart@uu.nl, b.g.ruessink@uu.nl

[2]Applied Physics Department, Universitat Politècnica de Catalunya, Spain. daniel.calvete@upc.edu, francesca.ribas@upc.edu

bores create extra sediment re-suspension in the inner surf zone, in such a way that depth-integrated sediment concentration increases in the landward direction in that region. Rollers have a secondary effect on growth of finger bars via the roller radiation stresses in the momentum equation (similar to the effect of wave radiation stresses). For highly oblique waves, radiation stresses promote the required offshore current deflection over the up-current finger bars, whilst for smaller angles of wave incidence they inhibit such offshore current perturbations and damp the instability.

Transverse finger bars are smaller than crescentic bars and rip current systems and the deviation of the flow around transverse finger bars is weaker so that finger bars have not an important impact on coastal evolution, neither on coastal safety. However, finger bars are the visible print of physical mechanisms that dominate the evolution of the morphology of the inner surf zone, a highly complex region. Studying their formation improves our understanding of the governing mechanisms in this region. In order to gain a deeper understanding of finger bar formation it is essential to further compare model results to observational data, and thereby there is the need to study finger bars in other beaches.

In this contribution we expand knowledge of transverse finger bars by examining a 4-year long data set of video images of the Gold Coast, Australia, where the persistent oblique incidence of the waves should be particularly beneficial to the formation of finger bars. Observations are described in section 2. We complement our data analysis with simulations using the linear stability analysis model by Ribas et al. (2012) to examine hypotheses arising from the data analysis (section 3).

## 2. Observations

### 2.1. *Study site and data*

The study site is the Surfers Paradise beach, at the Gold Coast, East Australia. Surfers Paradise is a 20 kilometers long, more or less continuous stretch of beach, extending from Burleigh Heads in the South to the outfall of the Nerang River in the north. The study site is a 3 kilometers long stretch of coastline, at the northern end of this beach. The coastline is aligned approximately north-south and the beach is composed of predominantly quartz sand with a median grain size of 250 $\mu$m. An Argus video system, consisting in four cameras spanning an 180$^o$ view of the coastline, is installed on top of a 100 m high building (Ruessink et al., 2009). The Argus data comprises a 4-year set of daily, low-tide time-exposure video images. The plan-view images are obtained from the oblique camera images using standard photogrammetric techniques (e.g., see Figure 1). The location of the camera system is used as zero of the alongshore position. The specific time period studied, from 1 November 1999 to 31 October 2003, covers four Australian summers and winters and corresponds to years where some bathymetric information is available.

Two bathymetric surveys of Surfers Paradise were performed during the study period, on 28 February 2001 and on 12 June 2002. The bathymetric measurements extend from the backside of the beach to about 800 meters offshore. Figure 2 shows the 2002 bathymetry and an example of bathymetric profile, corresponding to the cross-shore line located about 600 m south of the cameras. This is the bathymetric profile that will be used as model input in section 3 because an event of finger bars occurred just before the survey in that location. The nearshore zone of the Gold Coast was characterized by an outer alongshore bar located at around 200 m from the shoreline, and an inner terrace with the edge located at approximately 100 m from the shoreline, see Ruessink et al. (2009) for a more extensive account of sandbar dynamics.

The Gold Coast is relatively open, exposed to waves year-round. The long-term average offshore rms wave height for the Gold Coast is 0.81 m, with higher than average waves between January and May, corresponding to the Australian summer and the cyclone season. The annual wave climate is dominated by swell generated in the Southern Ocean and Tasman Sea that impacts the coast as small to medium size, moderate to long period oblique waves, from the south to south-east (Splinter et al. 2011). Hourly values of wave height and period measured at the closest buoy, the Gold Coast buoy, are used. Since this buoy is not directional, wave direction is measured at Brisbane offshore buoy, at 80-m depth, and is transformed to its value at 18 m-depth using Snell's law. We use the angle of wave incidence with respect to the shore-normal and positive (negative) values indicate that waves come from the south (north). Apart from providing directional information, the Brisbane wave recordings are used to fill up eventual measurement gaps in the Gold Coast buoy data. The wave conditions measured during the study period are shown in Figure 3.

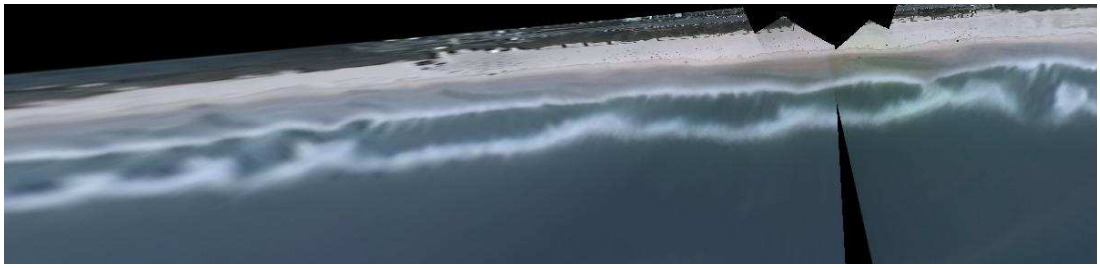

Figure 1. Example time-exposure image from the Gold Coast. The two white lines are the breaker zone over the (bottom) outer and (top) inner bar. Transverse finger bars can be seen attached to the inner bar as the small, obliquely oriented white stripes.

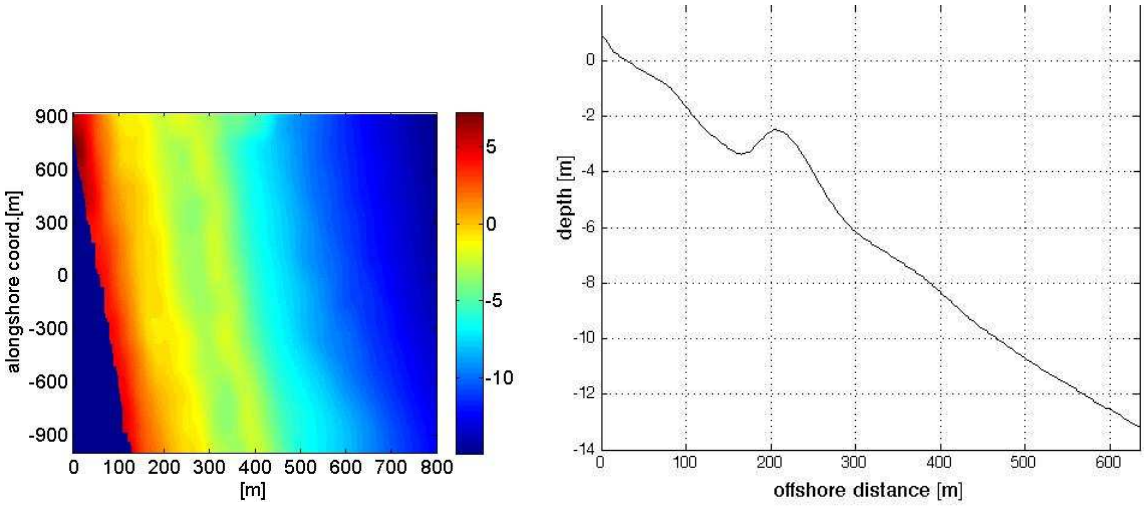


Figure 2. Bathymetric survey of Surfers Paradise on 12 June 2002 (left) and the bathymetric profile corresponding to the cross-shore line located about 600 m south of the cameras (right). The cross-shore positions in the two panels are measured with respect to a different origin.

### 2.2. *Analysis of observed finger bars*

The data set of Argus images from the study period is an almost continuous series of images: for 1430 days in total, there are only 59 days without any images of the beach. For every day of the study period, the plan-view images around daily low-tide were analyzed visually, tracking the occurrence of transverse finger bar events, their duration, the number of bars per event, the typical wavelength of the bars in a patch and the crest orientation and bar migration, both in a qualitative way. The occurrence of transverse finger bars is considered an event when a patch of 3 or more bars is visible for 2 or more days. 'Well developed' events are those in which a patch of 3 or more bars is visible for more than 2 days, or a patch of more than 3 bars is visible for 2 days (e.g., see Figure 1). The wavelength of finger bars in each patch were measured only for the well-developed events, as the alongshore averaged distance between bar crests (detected as maximum intensity locations due to preferable wave breaking over the finger bars). The wave conditions prior to the start of the events and the beach states were also analyzed for the well-developed events.

Patches of finger bars (that were part of an event) were observed during 24% of our study period. Typically, patches comprised 3 to 15 bars attached to the low-tide terrace, with average event duration of 5 days (an event with a maximum duration of 21 days was observed in March-April 2003). There was not a seasonal signal in the manifestation of finger bar presence (Figure 3). The alongshore wavelength varied from 17 to 71 m, with a data-set average value of 32 m. In most of the events (71%), finger bars were

oriented towards southeast (e.g., see Figure 1) and, in 27% of the bar patches, they pointed towards northeast. Finger bar patches at Surfers Paradise did not seem to migrate significantly along the coast and quantitative migration rates were not evaluated.

The ranges of wave conditions during the study period were root-mean-square heights ($H_{rms}$) varying from 0.2 to 2.86 m, peak periods ($T_p$) from 3 to 22.5 s, and absolute values of the wave angle ($\theta$) from 0 to 85°, with a clear dominance of southern waves (85% of the time) (Figure 3). The wave conditions prior to the formation of finger bars were analyzed by averaging these three quantities 24 hours before the moment when finger bars became visible in the images for the first time in each event. The $H_{rms}$ prior to the events never exceeded 1.2 m, with an average of 0.7 m, and the $T_p$ varied from 5.5 to 13 s, with an average of 9 s, indicating finger bars to be low to intermediate wave-energy features. The dominant angle of incidence measured with respect to the shore normal prior to bar formation had an average value of 28° and a standard deviation of 16°, and mainly corresponded to waves from southern directions. Orientation of bar crests was also quantitatively compared with the angle of wave incidence prior to the formation, showing that finger bars were typically up-current oriented. In 86% of the events where bars pointed towards the southeast, waves were coming from southeastern directions. In 79% of the events where bars were oriented towards the northeast, waves were coming from northeastern directions (in this latter case, comparison was done with the angles measured by the offshore buoy).

The beach states occurring most frequently when finger bars were present (43% of the time), were characterized as a rhythmic low-tide terrace (with alongshore variability at the length scales of a few hundreds of meters, similar to length scales in the outer bar (Price and Ruessink, in press)) and an undulating outer bar (either in a transverse bar and rip or in a rhythmic bar and beach state) (Figure 1). A detailed study of bar states at the Gold Coast is given in Price and Ruessink (2011). The finger bars were nearly always observed in the shoreward pointing embayments in the low-tide terrace, and rarely at the seaward directed perturbations of the terrace.

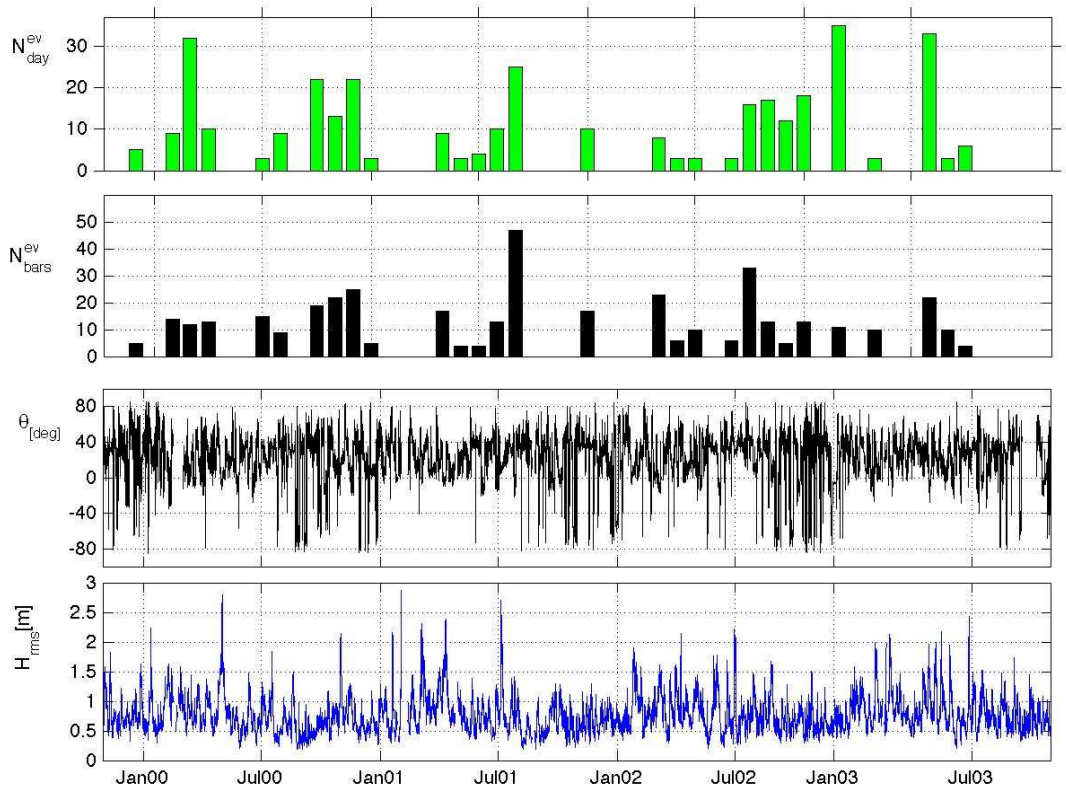


Figure 3. Monthly statistics of finger bar occurrence (first panel: number of days with finger bar patches; second panel: number of bars per month), angle of wave incidence from the shore-normal (third panel), were positive values mean waves from the south, and rms wave height (fourth panel).

## 3. Numerical simulations

### 3.1. *Model equations*

The model Morfo62 (Ribas et al., 2012) describes the feedback between wave and roller dynamics, depth-averaged currents and bed evolution. The $y$ (or $x_2$) axis is chosen to coincide with the rectilinear shoreline, the $x$ (or $x_1$) axis points in the seaward direction and the $z$ axis points upwards. A summary of the model equations are described below.

The model consists of depth- and time-averaged equations of continuity (1) and momentum (2), and therefore depth-uniform currents, along with a wave dispersion relation (3), a wave energy transformation (4), a roller energy transformation (5), and a bottom evolution equation (6), which follows from conservation of sediment mass. The resulting system of equations is

$$\frac{\partial D}{\partial t}+\frac{\partial}{\partial x_j}\left(Dv_j\right)=0 \qquad j=1,2 \tag{1}$$

$$\frac{\partial v_i}{\partial t}+v_j\frac{\partial v_i}{\partial x_j}=-g\frac{\partial z_s}{\partial x_i}-\frac{1}{\rho D}\frac{\partial}{\partial x_j}\left(S_{ij}^{w}+S_{ij}^{r}-S_{ij}^{t}\right)-\frac{\tau_{bi}}{\rho D} \qquad i,\,j=1,2 \tag{2}$$

$$\Omega_w=\sqrt{g\left|\vec{K}\right|\tanh\left(\left|\vec{K}\right|D\right)}+v_jK_j \qquad j=1,2 \tag{3}$$

$$\frac{\partial E}{\partial t}+\frac{\partial}{\partial x_j}\left(\left(v_j+c_{g\,j}\right)E\right)+S_{jk}^{w}\frac{\partial v_k}{\partial x_j}=-\mathsf{D}_w \qquad j,k=1,2 \tag{4}$$

$$\frac{\partial\left(2E_r\right)}{\partial t}+\frac{\partial}{\partial x_j}\left(2\left(v_j+c_j\right)E_r\right)+S_{jk}^{r}\frac{\partial v_k}{\partial x_j}=-\mathsf{D}_r+\mathsf{D}_w \qquad j,k=1,2 \tag{5}$$

$$(1-p)\frac{\partial z_b}{\partial t}+\frac{\partial q_j}{\partial x_j}=0 \qquad j=1,2 \tag{6}$$

Here, $D = z_s - z_b$ is the water depth, where $z_s$ is the free surface elevation and $z_b$ is the sea bottom level, $v_j$ are the two components of the depth-averaged water velocity, $g$ is gravity, $\rho$ is the water density, $\tau_{bi}$ are the bed shear stresses, and $S^{w}_{ij}$, $S^{r}_{ij}$, and $S^{t}_{ij}$, are the wave, roller and turbulence induced radiation stresses, respectively. Furthermore, $K_j$ are the two components of the wave number, $\Omega_w$ is the absolute wave frequency, $E$ and $E_r$ are the wave and roller energy densities, $\mathcal{D}_w$ and $\mathcal{D}_r$ are the wave and roller energy dissipation rates, $c_{gj}$ and $c_j$ are the group and phase velocity components, $p = 0.4$ is the porosity of the bed and $q_i$ are the two components of the wave-averaged volumetric sediment transport ($m^2/s$).

The bed shear stresses, $\tau_{bi}$ in equation (2), are parameterized following the generalized equation developed by Feddersen et al. (2000), extended to model the effect of a 2-dimensional flow. The corresponding drag coefficient $c_D$ is assumed to vary with depth following the Manning-Strickler law (Soulsby 1997), where the bed roughness, $k_a$, is constant and its default value (Table 1) is within the range of realistic values (Ruessink et al., 2001). The turbulent Reynolds stresses, $S^{t}_{ij}$ in equation (2), are modeled with the standard eddy viscosity approach. The lateral turbulent mixing coefficient is directly linked to the roller energy dissipation rate (the main source of turbulence), $\upsilon_t = M\,(\mathcal{D}_r/\rho)^{1/3}$, where $M = 1$.

Table 1. Default parameter setting, where the values for the offshore wave conditions lie close to the mean values measured during the finger bar events at Surfers Paradise.

| Parameter | Meaning | Value |
|---|---|---|
| $k_a$ | Apparent bed roughness | 0.035 m |
| $\gamma_b$ | Coefficient of saturation in $D_w$ | 0.475 |
| $d_{50}$ | Sediment grain size | 0.25 mm |
| $n_{rol}$ | Roller-induced stirring parameter | 50 |
| $H^{off}$ | Offshore rms wave height | 0.8 m |
| $\theta^{off}$ | Offshore wave incidence angle | 30° |
| $T_p$ | Peak wave period | 7.5 s |

Waves are assumed to have a narrow spectrum in frequency and angle. Their heights are supposed to be random and follow the Rayleigh distribution, characterized by the root mean square wave height, $H_{rms}$ (wave energy density being $E = \rho g H^2_{rms}/8$). For brevity, we denote $H_{rms}$ as $H$ from now on. Linear wave theory yields the dispersion relation (3), and expressions for wave properties such as their radiation stresses, $S^w_{ij}$, the root mean square wave orbital velocity amplitude near the bottom, $u_{rms}$, and the two components of the group and phase velocity, $c_{gi}$ and $c_i$. Steady conditions are assumed, $\Omega_w$ = constant. Applying wavenumber irrotationality, equation (3) is finally rewritten in terms of the wave phase $\Phi$, from which $K_i$ and $\Omega_w$ can be computed. The wave incidence angle with respect to the shore-normal, $\theta$, is computed from $K_i$ and the peak wave period, $T_p$, is computed from $\Omega_w$. The energy dissipation rate due to wave breaking, $\mathcal{D}_w$ in equation (4) and (5), is parameterized following Thornton and Guza (1983). We assume that the fraction of broken waves is $B$ = 1, which means that the entire front of the waves is covered with foam, consistent with the derivation of the roller equations. The value used for the saturation ratio of *H/D* (Table 1) is within the range of recommended values (Thornton and Guza, 1986). Equations (3) and (4) describe the refraction of the waves due to both topography and currents, together with wave breaking. More complex processes in wave propagation (e.g., wave diffraction) are not accounted for. The energy dissipated by breaking feeds the surface rollers, i.e. the aerated mass of water located on the shoreward face of breaking waves. The wave- and depth-averaged roller energy balance (5) is an extension of the one proposed by Reniers et al. (2004). The roller radiation stresses, $S^r_{ij}$, are computed following Svendsen (1984). The roller energy dissipation rate, $\mathcal{D}_r$, is modeled following Ruessink et al. (2001), with a standard value for the slope of the roller/wave front, $\beta$ = 0.05.

A widely accepted formulation for the sediment transport in the nearshore, $q_i$ in equation (6), is that of Soulsby and van Rijn (Soulsby, 1997), SvR-formula from now on. Their original expression has been extended to model the effect of a 2-dimensional flow and the preferred downslope transport of the sand,

$$q_i = C_{di}\left(v_i - \Gamma\frac{\partial h'}{\partial x_i}\right) \qquad i = 1,2 \tag{7}$$

where $C_{di}$ is the depth-integrated volumetric sediment concentration, $\Gamma$ is the bedslope coefficient, and $h'$ is a small perturbation of the bed level. We have extended SvR-formula to include the contribution to $C_{di}$ due to the stirring of sediment created by the bore induced turbulence, following Reniers et al. (2004),

$$C_{di} = A_s\left(\left(|\vec{v}|^2 + \frac{0.018}{c_D}u^2_{rms} + n_{rol}u^2_{rol}\right)^{0.5} - u_{crit}\right)^{2.4} \tag{8}$$

where $u_{crit}$ is the threshold flow intensity for sediment transport, the parameter $A_s$ accounts for the sediment properties, $u_{rol}$ is a representative turbulence velocity of the vortices created after roller energy is dissipated and $n_{rol}$ is a constant parameter. In the original SvR-formula, $C_{di}$ was assumed to be a result of the shear stresses produced in the bottom boundary layer of the wave orbital velocity and the depth-averaged currents (first two terms inside the square root of equation (8)). The SvR-formula was tested to be accurate in the shoaling domain, at water depths of the order of 5 m (Soulsby, 1997). However, in the inner surf zone (depths < 1 m), where $u_{rms}$ and the longshore current decay, other processes like bore propagation and

the created turbulence also produce significant sediment resuspension (Voulgaris and Collins, 2000). In the present study, the third term inside the root square in equation (8) has been added to allow inclusion of this other possible process. Here, the formulation of Roelvink and Stive (1989) is adopted, i.e., this extra $u_{rol}$ is assumed to depend on the dissipation of roller energy,

$$u_{rol} = \left( \frac{\mathsf{D}_r}{\rho} \right)^{1/3} \left( e^{(D/H)} - 1 \right)^{-1/2} \tag{9}$$

By varying $n_{rol}$ in equation (8) we can change the strength of the sediment stirring due to roller-induced turbulence. A default value $n_{rol} = 50$ is used, which gives reasonable values of $C_{di}$ of about $5 \cdot 10^{-3}$ m in the inner surf zone. The original SvR-formula is obtained for $n_{rol} = 0$. The Manning-Strickler law is again assumed for the drag coefficient $c_D$ and the full expressions for $u_{crit}$ and $A_s$ are given in Soulsby (1997). The bedslope term in equation (7) accounts for the tendency of the system to smooth out the sea bed perturbations, $h'$, if they do not cause positive feedback into the flow. The coefficient $\Gamma$ has also been extended to include the effect of the surface rollers. The values used for the corresponding parameters yields bedslope coefficients similar in magnitude to those of the original SvR-formula (Soulsby, 1997).

The equations (1)-(6), together with the described parameterizations, define a closed dynamical system for the variables $v_1$, $v_2$, $z_s$, $E$, $E_r$, $\Phi$ and $z_b$. The fluid velocities are imposed to vanish at both the coastline and the offshore boundary, were we also assume a fixed bed level. Also, the free surface elevation and $E_r$ are assumed to vanish at the offshore boundary, where wave conditions are prescribed ($H^{off}$, $\theta^{off}$ and $T_p$). The offshore boundary is at the location of the Gold Coast buoy (18-m depth).

The stability analysis approach to the formation of bars by self-organization starts by defining a steady and alongshore uniform basic state (i.e., without alongshore rhythmic topography). In this study, we used an alongshore uniform bathymetry characterized by the reference profile, $z_b^o(x)$, measured at the Gold Coast soon after a finger bar patch was observed (Figure 2b), with a low tide terrace and an outer alongshore bar. The modeled basic state solution consists of an alongshore current, $v^o_1 = 0$ and $v^o_2 = V^o(x)$, and an elevation of the mean sea level, $z_s^o = z_s^o(x)$ (Figure 4). This basic state only represents morphodynamic equilibrium if the net cross-shore sediment flux vanishes. The superscript $^o$ denotes the basic state variables.

Once the basic state has been computed, linear stability analysis is applied. A small perturbation, assumed to be periodic in time and in the alongshore coordinate, is added to this state,

$$(v_1, v_2, z_s, E, E_r, \Phi, z_b) = (0, V^o, z_s^o, E^o, E_r^o, \Phi^o, z_b^o) + \Re e\left\{ e^{(\omega t + i\kappa y)} (u, v, \eta, e, e_r, \phi, h) \right\} \tag{11}$$

where $\kappa$ is the alongshore wavenumber and $\omega$ a complex growth rate. Expression (11) is inserted in the governing equations (1)-(6), which are subsequently linearized with respect to the perturbations. As a first step, the perturbations of the depth-integrated sediment concentration, $C_{di}$, and the roller radiation stresses, $S^r_{ij}$, are neglected because spurious numerical solutions appear otherwise. The linearized equations lead to an eigenproblem in which different eigenvalues $\omega$ exist for each $\kappa$ (characterizing different solutions) and the complex eigenfunctions are $(u(x), v(x), \eta(x), e(x), e_r(x), \phi(x), h(x))$. The growth rate of the emerging bars is given by $\Omega = \Re_e(\omega)$, so that $\Omega > 0$ means growth. In case of an unstable basic state, solutions with $\Omega > 0$ are found and the growth rate curves show these positive $\Omega$ for different values of $\kappa$. Starting from arbitrary initial conditions, the dynamics after some time will be dominated by the mode with largest growth rate, which is called Fastest Growing Mode (FGM). Its $e$-folding growth time is given by $T_g = \Omega^{-1}$ and its migration speed by $c = -\Im_m(\omega)/\kappa$. The alongshore wavelength of the corresponding bar patch is $\lambda = 2\pi/\kappa$ and the shape of the final topography and the associated quantities are given by equation (11).

### 3.2. *Model results*

The basic state solution obtained for the default parameter setting (Table 1) consisted of a wave height profile, $H^o$, showing dissipation over the alongshore bar and at the terrace edge (Figure 4). Correspondingly, peaks of the alongshore current, $V^o$, and the depth-averaged concentration, $C^o_{di}$, occur near these two locations. Note that $C^o_{di}$ decreases from the terrace edge towards the seaward direction. This effect, essential for the growth of up-current finger bars, is caused by the sediment re-suspension by rollers.

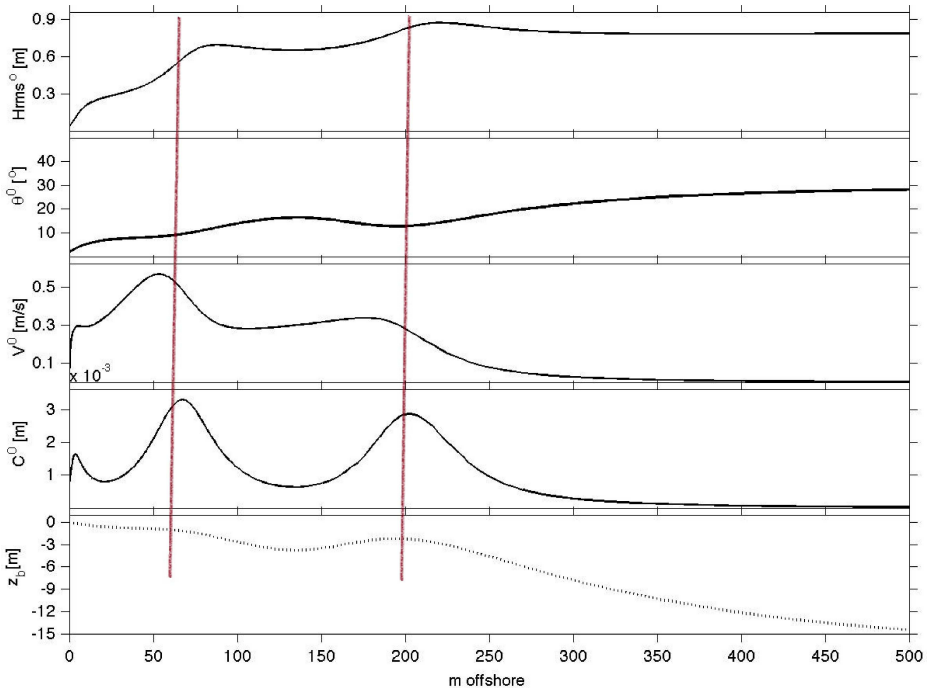


Figure 4. Basic state solution corresponding to the default parameter setting: cross-shore distribution of the wave height (first panel), wave incidence angle (second panel), alongshore current (third panel), depth-integrated concentration (fourth panel), and bathymetric profile (fifth panel). Vertical red lines indicate the terrace edge and the outer bar crest.

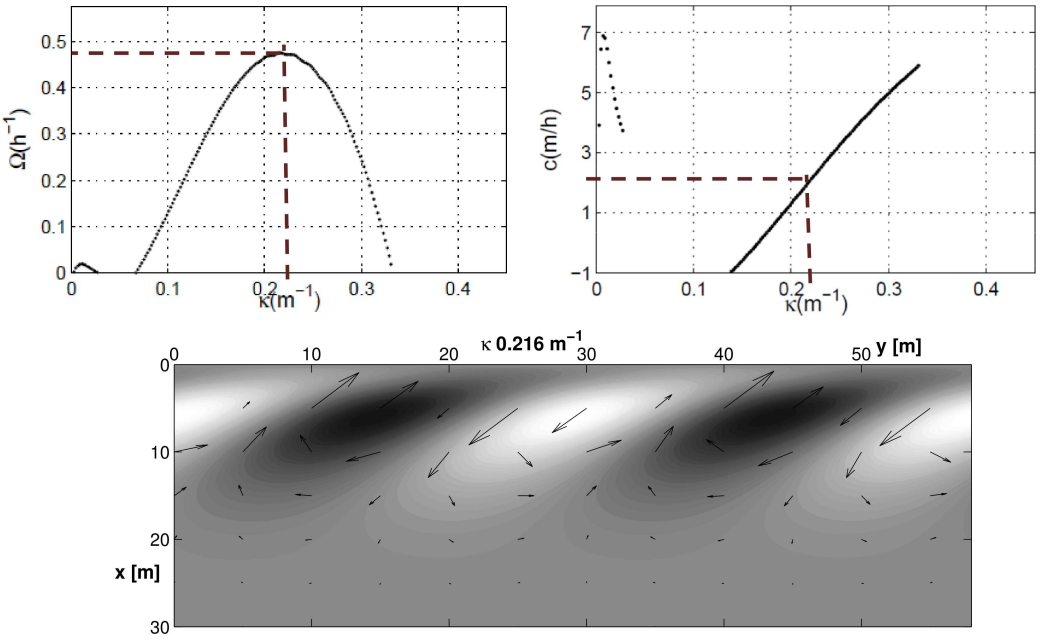


Figure 5. Growth rate Ω versus wave number of the perturbation κ (top left) and migration rate Ω versus wave number of the perturbation κ (top right) for the default parameter setting. Topographic and current perturbations corresponding to the Fastest Growing Solution (bottom), where white areas indicate bar crests and darker areas represent troughs. Waves come from the bottom left corner, so bars are up-current oriented. The arrows represent the perturbation of the current velocities, showing seaward directed flow over the crests and shoreward directed flow in the troughs.

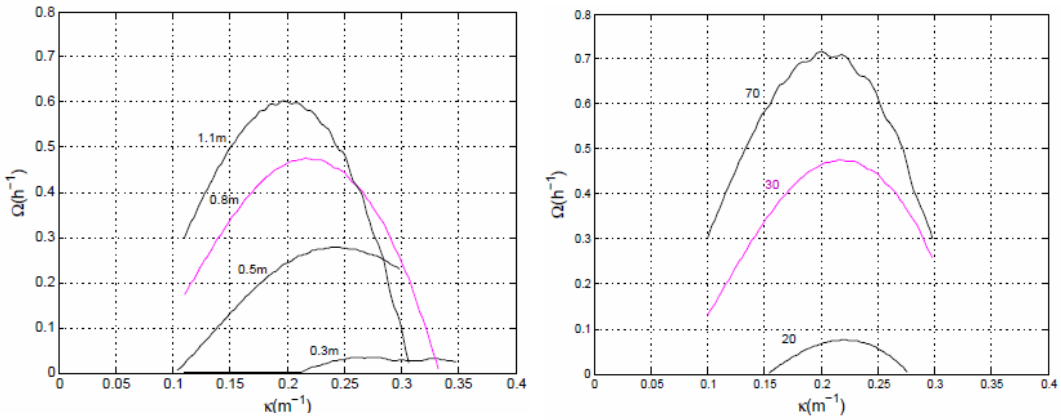


Figure 6. Growth rate Ω versus wave number of the perturbation κ for varying offshore wave height (left) and angle of incidence (right). The purple line indicates the result for the default parameter setting.

The linear stability analysis corresponding to the default parameter setting (i.e., using the wave conditions averaged over all finger bar events), produced one dominant growing solution consisting of a patch of up-current finger bars with an alongshore wavelength of 29 m (Figure 5). The angle that the crests make with the shore normal was larger than in the observations. The predicted maximum growth rate was 0.49 $h^{-1}$, corresponding to an e-folding growth time of 6 hours. The modeled migration rate of this bar patch was 1.9 m $h^{-1}$, whilst bars seemed not to migrate significantly in the observations. Seaward (shoreward) directed flow perturbations were obtained over the crests (troughs) of the finger bars.

Simulations in which the offshore wave conditions were varied revealed that transverse finger bars formed when the offshore wave height was larger than 0.3 m and the offshore wave angle was larger than 20°. In general, higher growth rates were found for higher waves and for increasing the angle of wave incidence up to 60° (Figure 6). Predicted wavelength slightly varied (20%) when varying wave conditions and modeled migration rates increased for larger $H^{off}$ and $\theta^{off}$. From a process perspective, we observed that, according to the model, sediment re-suspension by roller-induced turbulence promoted the shoreward increase in depth-averaged sediment concentration necessary for transverse bars to form (i.e., growth rates increased with larger values of $n_{rol}$ parameter in equation (8)). For a fixed value of $n_{rol}$, the strength of the alongshore current (which increases for larger $H^{off}$ and $\theta^{off}$) determined the growth and migration rates.

## 4. Discussion and conclusions

The formation of transverse finger bars in the surf zone of Surfers Paradise beach, at the Gold Coast, East Australia, has been investigated with Argus video observations and an existing morphodynamic model based on linear stability analysis (called Morfo62).

The video data comprise a four-year (November 1999 - October 2003) set of daily, low-tide time-exposure video images and associated hourly records of offshore (in 18-m depth) wave height, period and direction. Transverse finger bars were observed during 24% of the study period, substantially more often than in the earlier observations from Duck and Noordwijk. They occurred in patches of 3 to 15 bars attached to the low-tide terrace, with an average lifetime of 5 days. The alongshore wavelength varied from 17 to 71 m, with a data-set average value of 32 m (similar to finger bars at Noordwijk). The offshore root-mean-square wave height prior to the formation of transverse finger bars never exceeded 1.2 m, indicating finger bars to be low to intermediate wave-energy features, as at Duck and Noordwijk. The dominant angle of wave incidence prior to formation of finger bars varied between 12 and 44° from shore normal. As this corresponded to waves from southern directions and most bar crests were oriented toward the south, finger bars were typically up-current oriented. Note that there is some uncertainty in determining the wave conditions prior to bar formation because video images do not allow to observe the initial steps of bar

formation (bars are visible in the images only when their amplitude is already significant). For this same reason, the characteristic growth time of finger bar formation can not be measured in the video images. An estimation of the growth time is the typical duration of the required wave conditions leading to bar formation, which is of the order of 1 day. In contrast with observations at Duck and Noordwijk, patches of finger bars at the Gold Coast were not observed to migrate. When finger bars were present, the width of the low-tide terrace often displayed alongshore variability of a few hundreds of meters, enforced by the variability in the onshore propagating outer bar. It remains unclear whether this beach state configuration actually influences finger bar formation because both this beach state and finger bars are features typical of low to intermediate wave conditions. Clearly, finger bars were typically observed in the shoreward pointing embayments of the low-tide terrace instead of at its seaward directed perturbations. This is consistent with observations at Noordwijk, where formation of finger bars only occurred when the distance between the shoreline and the alongshore bar was larger than a critical value. A meandering alongshore current is essential for finger bar formation and it requires a certain space to flow freely.

The Morfo62 model was used to examine the initial formation of transverse finger bars on an alongshore-uniform bathymetry with an outer bar and an inner low-tide terrace. With an offshore root-mean-square wave height, period and angle of incidence averaged over all finger bar events (0.8 m, 7.5 s and $30^o$, respectively), the model produced up-current finger bars attached to the low-tide terrace with an alongshore wavelength of 29 m, consistent with the observations. The predicted e-folding growth time was 6 h and the modeled migration rate was 1.9 m $h^{-1}$. Simulations in which the offshore wave conditions were varied revealed that transverse finger bars formed if the offshore wave height was between 0.3 and 1.2 m and the offshore wave angle varied between 20 and $85^o$. Growth rates increased when increasing the height and the angle of incidence of waves, because the strength of the alongshore current controls the growth rate of finger bars. According to the model, sediment re-suspension by roller-induced turbulence promoted the shoreward increase in depth-averaged sediment concentration necessary for transverse bars to form. The overall characteristics of finger bars observed at the Gold Coast, i.e., shape (wavelength, up-current orientation), growth rate and wave conditions leading to their formation, were relatively well reproduced by the model. However, both the values of the modeled migration rate and angle of crest orientation with respect to shore-normal were larger than observed values. This also occurred in the model-data comparison of finger bars at Noordwijk beach. The fact that finger bars at the Gold Coast were observed to coincide with rhythmic bar states can not be reproduced by the present model, based on linear stability analysis, which requires an alongshore uniform initial bathymetry.

Future work will focus on the sensitivity of the results to variations in the characteristics of the initial profile (e.g., shape and location of the outer longshore bar, beach-face slope, etc.). Another point of study will be to use a non-linear model to start with a more realistic initial bathymetry, incorporating pre-existing larger-scale variability. With this tool, it will be investigated how the formation of transverse finger bars is affected by the change from an alongshore-uniform current into a more meandering flow pattern.

## Acknowledgements

Funding from the Spanish research project `Modelización y monitorización integradas en morfodinámica de playas naturales y regeneradas' (contract CTM2009-11892) and from the Netherlands Organisation for Scientific Research NWO (contract 818.01.009) is acknowledged.

## References

Feddersen F., Guza R.T., Elgar S. and Herbers T.H.C., 2000. Velocity moments in alongshore bottom stress parameterizations. *Journal of Geophysical Research*, 105(C4): 8673–8686.

Konicki, K.M. and Holman, R.A., 2000. The statistics and kinematics of transverse bars on an open coast. *Marine Geology*, 169: 69-101.

Price, T.D., and Ruessink, B.G., 2011. State dynamics of a double sandbar system. *Continental Shelf Research*, 31: 659-674.

Price , T.D. and Ruessink, B.G., in press. Observations and conceptual modelling of morphological coupling in a double sandbar system. *Earth Surface Processes and Landforms*.

Reniers A.J.M.H., Roelvink J.A. and Thornton E.B., 2004. Morphodynamic modeling of an embayed beach under wave group forcing. *Journal of Geophysical Research*, 109(C01030): doi:10.1029/2002JC001586.

Ribas, F. and Kroon, A., 2007. Characteristics and dynamics of surfzone transverse finger bars. *Journal of Geophysical Research*, 112: doi:10.1029/2006JF000685.

Ribas F., de Swart H.E., Calvete D. and Falqués A., 2011a. Modelling waves, currents and sandbars on natural beaches: the effect of surface rollers. *Journal of Marine Systems*, 88: 90-101.

Ribas, F., de Swart, H.E., Calvete, D. and Falqués, A., 2011b. Modelling the formation of transverse sand bars: application to Duck beach, USA. *Proc. 7th IAHR Symposiumn on River Coastal and Estuarine Morphodynamics (RCEM 2011)*.

Ribas, F., de Swart, H.E., Calvete, D. and Falqués, A., 2012. Modeling and analyzing observed transverse sandbars in the surf zone. *Journal of Geophysical Research*, 117 (F02013): doi:10.1029/2011JF002158.

Roelvink J.A. and Stive M.J.F., 1989. Bar-generating cross-shore flow mechanisms on a beach. *Journal of Geophysical Research*, 94(C4): 4785–4800.

Ruessink B.G., Miles J.R., Feddersen F., Guza R.T. and Elgar S., 2001. Modeling the alongshore current on barred beaches. *Journal of Geophysical Research*, 106(C10): 22451–22463.

Ruessink B.G, Pape L. and Turner, I.L., 2009. Daily to interannual cross-shore sandbar migration: observations from a multiple sandbar system. *Continental Shelf Research*, 29, 1663-1677.

Soulsby R.L., 1997. *Dynamics of Marine Sands*. London, U.K.: Thomas Telford.

Splinter, K. D., Strauss, D. R., and Tomlinson, R.B., 2011. Assessment of post-storm recovery of beaches using video imaging techniques: a case study at Gold Coast, Australia. *IEEE Transactions on Geoscience and Remote Sensing*, 49(12):4704-4716.

Thornton E.B., and Guza, R.T., 1983. Transformation of wave height distribution. *Journal of Geophysical Research*, 88(C10): 5925–5938.

Thornton E.B., and Guza, R.T., 1986. Surf zone longshore currents and random waves: field data and models. *Journal of Physical Oceanography*, 16: 1165–1178.

Svendsen I. A., 1984. Wave heights and setup in the surf zone. *Coastal Engineering*, 8: 303–329.

Voulgaris G., and Collins M.B., 2000. Sediment resuspension on beaches: response to breaking waves. *Marine Geology*, 167: 167–187.